УДК 691.542
DOI 10.22213/2410-9304-2018-3-169-178

ELECTRODEPOSITION-ANODIZATION PREPARATION OF NANOCRYSTALLINE NICKEL FERRITE FILMS FROM AQUEOUS SULFATE SOLUTIONS: A MATERIAL FOR SENSING OF TOXIC HOUSEHOLD GASES AND HEALTH MONITORING

E. M. Elsayed, Central Metallurgical Research and Development Institute (CMRDI), Helwan, Egypt, elsayed2021@gmail.com
M. M. Rashad, CMRDI, Helwan, Egypt,
M. M. Moharam, CMRDI, Helwan, Egypt,
M. R. Hussein, Chemistry Department Faculty of Science, Al–Azhar University, Nasr City, Egypt
M. M. B. El-Sabbah, Chemistry Department Faculty of Science, Al–Azhar University, Nasr City, Egypt
I. A. Ibrahim, CMRDI, Helwan, Egypt

Nanocrystalline spinel nickel ferrite $NiFe_2O_4$ thin film has been studied and synthesized via the electrodeposition-anodization process. Electrodeposited $NiFe_2$ alloys were obtained from aqueous sulphate bath. The formed alloys were electrochemically oxidized (anodized) in aqueous (1 M KOH) solution, at room temperature, to the corresponding hydroxides and annealed in air at 400 ^{0}C for 2 h. The parameters controlling of the electrodeposition of $NiFe_2$ alloys such as the bath temperature, agitation and the current density were optimized. The crystal structure, crystal size and microstructure of the produced ferrites were investigated using X-ray diffraction (XRD) and scanning electron microscopy (SEM). XRD shows that $NiFe_2O_4$ had a spinel structure and. The crystallite size of $NiFe_2O_4$ phase was 16 nm. SEM micrograph of the formed ferrite particles shows that the distorted rectangular structure and semi square like morphology was noted.

Keywords: Nickel Ferrite, Electrodeposition, Anodization, Thin film, Cyclic voltammetry, Nanoparticles.

1. Introduction

There is a growing interest in magnetic ferrite nanoparticles because of their wide applications in Permanent magnets, magnetic drug delivery, microwave devices and high density information strong technology [1-4].

Spinel ferrites, MFe_2O_4, are technologically important group of materials due to their enhanced optical, magnetic, and electrical properties. These properties make them very attractive for a variety of applications including but not limited to use as electrodes in energy storage devices, as catalysts, in magnetic storage devices, etc. [5-7].

Spinel ferrites have the general formula of MFe_2O_4 (where M^{2+}: Cu, Co, Ni, Zn, etc.) and unit cell contains 32 oxygen atoms in cubic close packing with 8 tetrahedral (Td) and 16 octahedral (Oh) occupied sites. By changing type of the divalent cation, it is possible to obtain significantly different physical and magnetic properties in these ferrites [7].

Magnetic ferrites are a group of technologically important magnetic materials. Synthesis of nanocrystalline spinel ferrite has been investigated intensively in recent_years due to their potential applications in high-density magnetic recording, microwave devices, and magnetic fluids [8, 9]. Nickel ferrite has to be a good sensor to detect oxidizing gases like chlorine [10-12]. Nickel ferrite ($NiFe_2O_4$) is one of the most important spinel ferrites as well as a typical spin soft- magnetic ferrite. Various methods have been developed to synthesize nanocrystalline $NiFe_2O_4$ such as mechanical alloying [13], pulsed wire discharge [14], sol–gel method [15], microemulsion [16], hydrothermal-microwave [17] and hydrothermal processes [18]. Among these established methods, electrochemical synthesis has attracted great interest because it offers many advantages, including the formation of oxide films is economical and suitable for large-scale applications [16, 19]. Electricity accomplishes the oxidation and reduction, so that there are no by product species [16]. The method has low processing temperature and its low cost of raw materials or equipment. It controls the film composition and morphology using the electrochemical parameters. It is ability to deposit a film on a complex surface. This method is the easiest, non-vacuum method for preparing large area electrodes [17]. Homogeneous fine and reproducible nanocrystalline films are obtained [20-22].

In this paper, we report the synthesis of nano structured nickel ferrite thin film by the electrochemical deposition from the aqueous solution of sulphate bath and investigates the effect of synthesis condition such as agitation, temperature, current density, and deposition voltage on the properties of ferrite film to obtain the optimum conditions.

2. Materials and Methods

Analytical grade ammonium ferrous sulphate (Fe $(NH_4)_2$ $(SO_4)_2$.6 H_2O), nickel sulphate ($NiSO_4$ 6 H_2O) and potassium hydroxide (KOH) were used as starting materials. Electrodeposition experiments were carried out using freshly prepared solutions. The electrolyte was kept unstirred.

The cell

The experimental set-up is shown in Fig. 1. A standard three-electrode cell (40 cm^3) in which 2 Pt plates were used as working and auxiliary electrode. The area of these two electrodes was 1 cm^2. The reference electrode used was a saturated silver /silver chloride electrode ($Ag/AgCl_{sat}$), $E_0 = 0.200$ mV vs. standard hydrogen electrode (SHE) reference electrode. The working and the counter electrodes were mounted parallel to each other at a distance of 0.5 cm.

Electrocodeposition of nickel iron alloy: Experiments of electrodeposition were executed using a potentiostate- galvanostate (25 V/3A) in a galvanostatic mode. Just before deposition, the working electrode was anodically cleaned for 60 s at a current density of 0.01 A cm^{-2} in a bath similar to that used for alloy deposition.

In a second step, the deposited nickel iron alloy film was anodized in 1 M KOH where the alloy film acts as anode and the counter Pt- electrode acts as cathode. The resulting film was rinsed thoroughly with distilled water and dried under vacuum in desiccators for at least 2 h.

Fig. 1. Experimental set-up

Cyclic voltammetric (CV) tests were performed at room temperature using previous mentioned three-electrode cell, in which Pt was used as working electrode and auxiliary electrode. The deposition potentials were determined from the polarization curves. Cyclic voltammograms were performed with a computer-controlled potentiostat (Volta-lab 21). Cyclic voltammograms were accomplished with a computer-controlled potentiostat (Volta- lab 21). PGP 201 potentiostate, Galvanosatate 20V, 1A with general generator.

Electrodeposition was identified galvanostatically using constant currents ranging from -10 to -100 mA. Apparent current densities were obtained by dividing the applied current by macroscopic surface area of the deposit. The deposition conditions were optimized to get good quality of $NiFe_2$ alloy films with maximum thickness.

The alloy films were anodized using aqueous 1M KOH. The anodization current density and time were optimized to get well-adhered oxide films to the substrates. After anodization, the films were washed with distilled water and annealed after drying.

The crystalline phase in the different annealed ferrite samples was investigated using X-ray diffraction (XRD) on a Brucker axis D8 diffractometer using the Cu-Kα(λ = 1.5406 A$^\circ$) radiation and secondary monochromator in the range 2θ from 20° to 80°. The ferrite particle morphologies were examined by Scanning Electron Microscope (SEM) (JEOL—model JSM-5410). The crystallite size was calculated automatically by the X –ray diffractometer.

Results and Discussion

Cyclic Voltammetry (CV)

Figures 2a, b, c showed the cyclic voltammogram (CV) of 0.05 M of $NiSO_4$, 0.1 M Fe $(NH_4)_2$ $(SO_4)_2$ and $NiFe_2$ alloy, respectively, from aqueous sulfate bath. Voltammetric studies were performed within the range of 0 to −2 V using a scan rate (S.R.) of 10 mVs^{-1}. The CV of 0.05 M of $NiSO_4$ is given in Fig. 2a. It is investigated by one cathodic peak (C) at potential -1.18V. This cathodic peak is associated with the deposition of Ni^{+2} ions to metallic nickel.

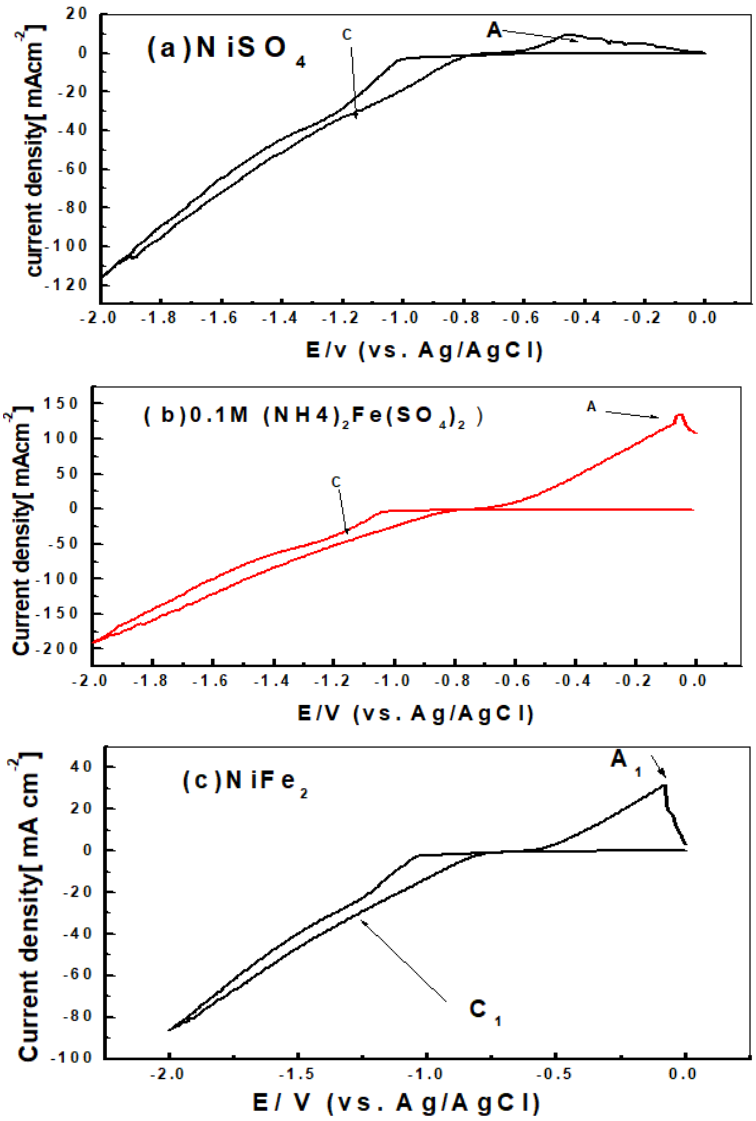

Fig. 2. Voltammograms obtained on Pt electrode in aqueous solution of: **a** 0.05M $NiSO_4$, **b** 0.1M $(NH_4)_2Fe(SO_4)_2$ and **c** $NiFe_2$ alloy deposited from solution of 0.1 M Fe $(NH_4)_2$ $(SO_4)_2$ +0.05M $NiSO_4$

Alongside, on reversing scan in positive direction at -2 V, an anodic peak (A) was appeared around potential -0.38 V for non-stirred solution. This anodic peak represents the dissolution of Ni metal into Ni^{+2} ions according to the following equation (1):

$$Ni + 2 + 2e - \leftrightarrow Ni \qquad (1)$$

Fig. 2 (b) depicts the CV of 0.1M of Fe $(NH_4)_2(SO_4)_2$. Iron electrodeposition was started at potential -1.2V for non-stirred solution (peak C). Thus, this peak was corresponded to the electrodeposited of iron. This iron deposition process was reported to be sensitive to mass transfer [23]. However, on reversing scan in positive direction at -2 V, an anodic peak was appeared around -0.1 V (peak A). This anodic peak was reduced the dissolution of iron metal into its ions.

Fig.2(c) illuminates the CV of $NiFe_2$ alloy. $NiFe_2$ alloy is considered as anomalous iron alloy, because of the preferential deposition of the less noble metal in the presence of ferrous ion. Nickel reduction is inhibited while the iron deposition rate is enhanced compared with their individual deposition rates in single metal plating baths. Early theory in Fe-Ni electrodeposition suggested that the formation of Fe $(OH)_2$ on the surface is acting as selective membrane that inhibited the nickel reduction but permits iron to be deposited [23]. It can be seen that one cathodic peak and one anodic peak were observed for $NiFe_2$ alloy. The first cathodic peak (C1) was detected at potential E = -1.2 V for non-agitated solution. This peak belongs to the co-deposition of $NiFe_2$ alloy. However, on reversing scan in positive direction at -2 V, an anodic peak (A1) was appeared around -0.1 V. This peak was due to the dissolution of the deposited alloy.

Effect of agitation

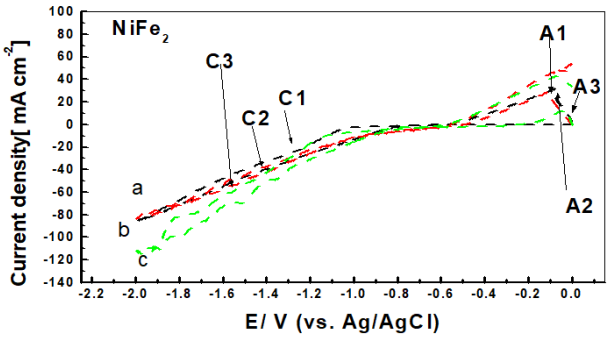

Fig. 3a. Voltammograms obtained on pt electrode in aqueous solution of $NiFe_2$ alloy, SR (10 mV/s), cycle: **a** 0rpm, **b** 500 rpm, **c** 1000 rpm deposited from solution of 0.1 M Fe $(NH_4)_2$ $(SO_4)_2$ + 0.05M $NiSO_4$

Fig. 3(a) represents the cyclic voltammeteric curves for electrodeposition of $NiFe_2$ alloy at different agitation conditions. The curves are characterized by three cathodic peaks C_1, C_2, C_3 respectively. The first cathodic peak C_1 appeared at potential -1.2 V at non agitated solution. On agitating the solution, 500 rpm, the co-deposition potential of the cathodic peak (C_1) was shifted to (C_2) at potential -1.48 V and the current density was shifted from -82 to -84 mA cm^{-2}. Meanwhile agitating the solution from 500 to 1000 rpm is also shifted the current density from -84 to -115 $mAcm^{-2}$ while the co-deposition potential was shifted from -1.2V (C_1) to -1.524 V (C_3). $NiFe_2$ alloy is considered as anomalous alloys [23]. Moreover, agitating the solution changed the solution cathodic current density from -80 to -120 mA cm^{-2}. Increasing the solution agitation rate reduces the thickness of the adjacent cathodic layer, which in turn shortness the diffusion path of the deposition of metals [24, 25]. However, on reversing scan in positive direction at -2 V, an anodic peaks (A1,A2,A3) appeared around. The anodic peak was due to the dissolution of the deposited alloy.

LSV for electrodeposition of $NiFe_2$ alloy

Effect of bath temperature

Fig.3 (b) illustrates the Linear sweep voltammeteric curves (LSV) for electrodeposition of $NiFe_2$ alloy on Pt substrate at different bath temperatures. It is found that, increasing bath temperature from 25 to 40^0C produced a decrease in $NiFe_2$ deposition potential from E = -1.52V, (peak C_1) to E = -1.4V, (peak C_2). Additionally, the increasing bath temperature from 40 to 60 ^{0}C was resulted in a decrease in $NiFe_2$ deposition potential from E = -1.4 V, (peak C_2) to E = -1.3 V, (peak C_3).

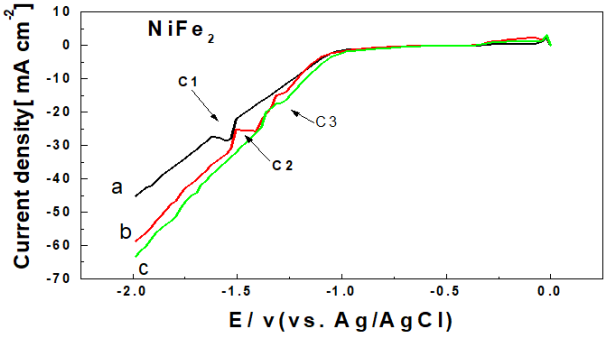

Fig. 3b. Linear sweep voltammeteric curves obtained on pt electrode in aqueous solution of $NiFe_2$ alloy, SR (10 mV/s), cycle: **a** 25 ^{0}C, **b** 40 ^{0}C, **c** 60 ^{0}C deposited from solution of 0.1 M Fe $(NH_4)_2$ $(SO_4)_2$ + 0.05M $NiSO_4$)

Generally, the raise in bath temperature increases the grain size which has deposited material and consequently a decrease in deposition potential at a higher temperature was observed. Additionally, the increment of bath temperature enhances the rate of diffusion and ionic mobilites which enhances the conductivity of deposition bath. The decrease in deposition potential with increasing temperature might be due to the increase in the content of more noble metal in the deposited alloy [26].

Chronopotentimetric study

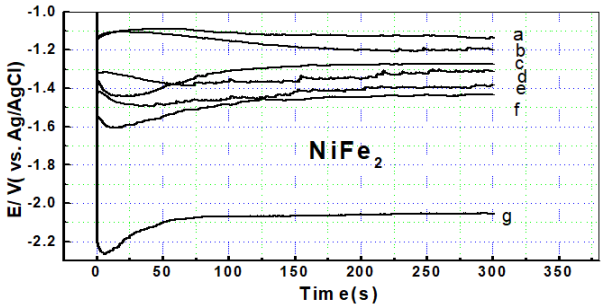

Fig. 4. Chronopotentiometric curves recorded at various current densities (**a** −10mA/cm^2, **b** −20mA/cm^2, **c** −30mA/cm^2, **d** −40mA/cm^2, **f** -50m/cm^2, **e** −60mA/cm^2, **g** −100mA/cm^2) in aqueous solution of $NiFe_2$ alloy deposited from solution of 0.1 M Fe $(NH_4)_2$ $(SO_4)_2$ + + 0.05M $NiSO_4$

Fig. 4 depicts the Chronopotentimetric (galvanostatic) curves for the electrodeposition of alloy containing $NiFe_2$ thin films from solution of 0.05 M $NiSO_4$ + 0.1 M Fe $(NH_4)_2$ $(SO_4)_2$. The depositions at different current values i.e. -10, -20, -30, -40, -50, -60 and -100 mA/cm^2 were performed respectively. The variation in the values of potential with time was noted. During the deposition, the potential first increases to a certain extent and then it decreases very fast up to a steady state value. The fast decrease in potential shows the coverage of electrode surface becomes fast whereas the steady state indicates that the coverage of electrode surface

is nearly complete. The value of deposition rate at current density (-100 mA/cm^2) was observed maximum with high film thickness. Thus, cathodic current density of -100 mA/cm^2 was found suitable for the deposition of thin films.

Chronoamperometric study

Fig. 5 displays the chronoamperometeric curve recorded with Pt substrate in the deposition solution of 0.05 M $NiSO_4$ + 0.1 M Fe $(NH_4)_2$ $(SO_4)_2$.

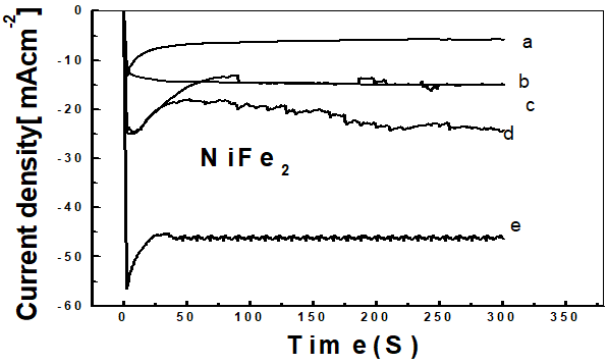

Fig. 5. Variation of current density with time at constant potentials (**a** 1V, **b** 1.1V, **c** 1.2V, **d** 1.3V, **e** 1.4V) for $NiFe_2$ deposited from solution of 0.1 M Fe $(NH_4)_2$ $(SO_4)_2$ + + 0.05M $NiSO_4$

During the early stage of deposition, the behavior of current density changes quit similarly, but after more than 60 s, the behavior differs. Immediately after potential application, the cathodic current rapidly increases, because nucleation starts and the three dimensional growth of each crystal rapidly increases the active surface area. The shape is typical for a three dimensional electrocrystallization growth process [27]. Moreover, the increase in deposition time (more than 60 s) causes a lowering in the current density to a constant plateau value. Hence during nucleation process, the electrochemical behavior depends on the applied potential; the current behavior becomes similar. This is imputed to the probability that the Pt substrate is completely covered by $NiFe_2$ layer.

The current is almost constant, with a value of about -10 mA cm^{-2} at the potential of -1.1, -20 mA cm^{-2} at a potential of -1.2 V, -25 mA cm^{-2} at a potential of -1.3 V and - 45 mA cm^{-2} at a potential of -1.4 V respectively. The value of deposition rate at -1.4V was observed maximum with high film thickness. Thus, potential -1.4 V was found to be a suitable for the deposition of thin films [28].

Scharifker and Hills suggested model to describe the nucleation process during initial few seconds using chronoamperometric technique [28]. The nucleation process may be either progressive or instantaneous. Progressive nucleation corresponds to slow growth of nuclei on a less number of active sites, all of these sites activated at the same time. Instantaneous nucleation corresponds to fast growth of nuclei on many active sites, all activated during the course of electroreduction. The effect of deposition potential on nucleation of alloy during initial time (S-H model) is shown in Fig. 6.a-d

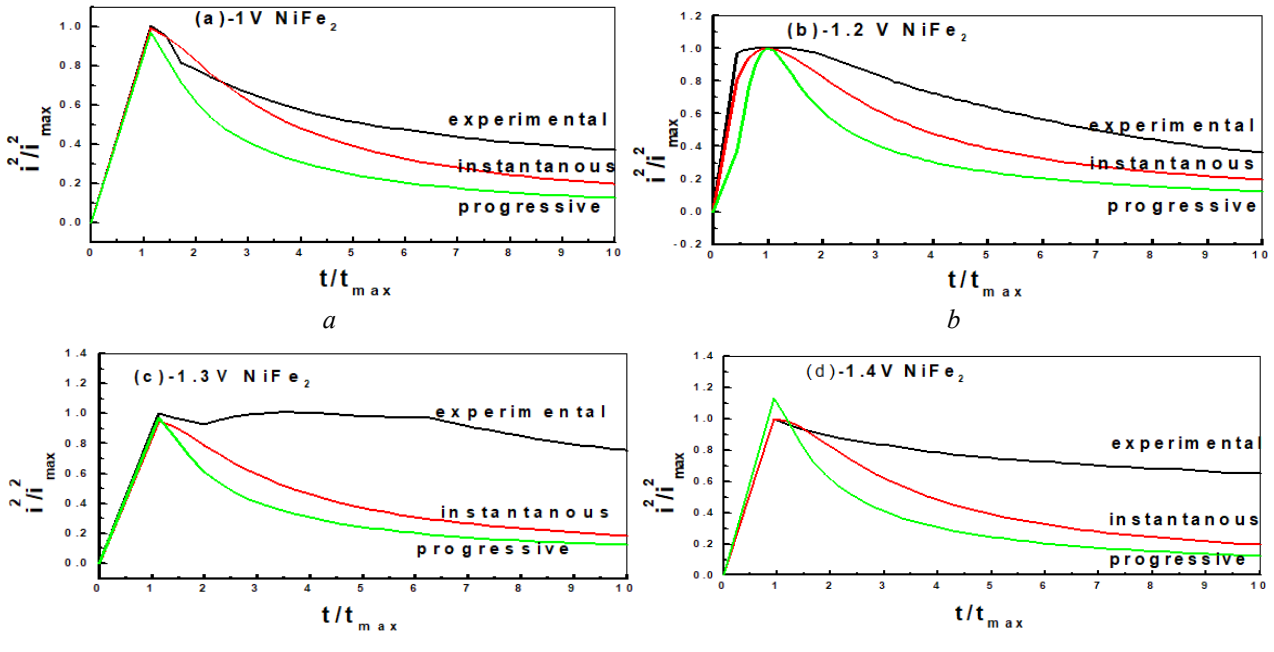

Fig. 6. Nondimensional i^2/i^2_{max} vs t/t_{max} plots for electrodeposited $NiFe_2$ alloy at different potentials
a -1V, **b** -1.2V, **c** -1.3V, **d** -1.4V

The transients have been analyzed by comparing the chronoamperometric curves to the dimensionless theoretical curves for the diffusion-controlled nucleation and growth of crystals in three dimensions (3D) proposed by Saba et al. (22; Saba et al. 2012).

The expressions for the instantaneous and progressive nucleation are given by following equations, respectively [29].

$$I^2/i_{max}{}^2 = 1{,}9542[t_{max}/t]\left(1-\exp[-1{,}2564\, t/t_{max}]\right)^2 \quad (2)$$

$$I^2/i_{max}{}^2 = 1{,}2254[t_{max}/t]\left(1-\exp[-2{,}3367(\, t/t_{max})^2]\right)^2 \quad (3)$$

Where i_{max} and t_{max} are the maximum current density observed at the maximum time t_{max}.

The fitting of the experimental curves for the theoretical curves are shown in Fig. 6 (a-d) for all potentials. The plots indicated that the nucleation and growth of $NiFe_2$ alloy electrodeposited from aqueous media were obeyed instantaneous mechanism.

Film Thickness measurements of $NiFe_2$ alloy

MFe_2 alloy film thickness was determined by the method of gravimetric weight difference in which area and weight of the film was measured, before and after alloy deposition [22, 30].

The samples were precisely weighed; the difference of two masses gives the mass of the alloy film. The thickness was obtained by assuming density of bulk MFe_2 expressed as:

$$T = mass\frac{difference}{\rho A} \quad (4)$$

$$\rho = \rho_1 x_1 + \rho_2 x_2 \quad (5)$$

Where ρ_1, ρ_2 and x_1, x_2 are densities and atomic fractions of M and Fe elements in alloy, respectively.

Fig. 7 shows the variation of film thickness with current density. Initially as current density increases, film thickness increases attains maximum value (3240 nm) for current density -100 mA cm^{-2}. Further increase in current density, the film splits off from the substrate. This is attributed to the formation of porous, foggy, less adherent film and/or the film may have tensile stress that tends to cause delamination, when it becomes thick.

The relation between film thickness and deposition potential is shown in Fig.8. It is observed that, initially as deposition potential increases, film thickness increases and attains maximum value 3400 nm at -1.4V deposition potential of $NiFe_2$.

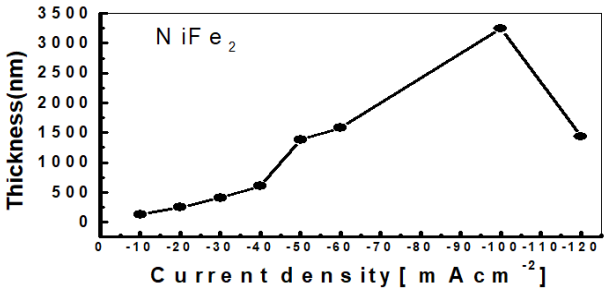

Fig. 7. Variation of film thickness with current density $NiFe_2$ alloy deposited from solution of 0.1 M Fe $(NH_4)_2$ $(SO_4)_2$ + 0.05M $NiSO_4$

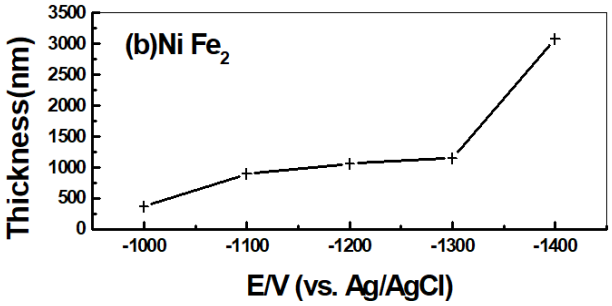

Fig. 8. Variation of film thickness with potential for $NiFe_2$ alloy deposited from solution of 0.1 M Fe $(NH_4)_2$ $(SO_4)_2$ + 0.05M $NiSO_4$

Current efficiency study of $NiFe_2$ alloy

Current efficiency was calculated by dividing the mass of the film actually deposited on the electrode by the mass expected to be deposited in accordance with Faraday's law.

$$W = \frac{Ix\,thrs\,x\,equivalent\,weight\,g}{26.8\,A.hr}\ \text{grams} \quad (6)$$

Where:

I – current intensity in Amperes.

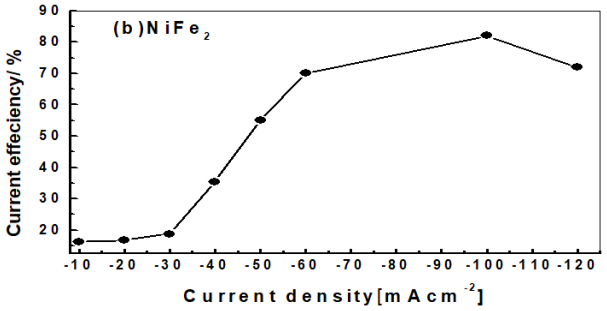

Fig. 9. Variation of current efficiency with current density for $NiFe_2$ alloy deposited from solution of 0.1 M Fe $(NH_4)_2$ $(SO_4)_2$ + 0.05M $NiSO_4$

Fig. 9 illuminates the relation between current density and current efficiency of $NiFe_2$ alloy**.** The results showed that the current efficiency increases initially with increasing the current density up to

-100 mA/cm^2 and decreases afterwards within the range studied. About 82 % current efficiency is obtained at current density of -100 mA/ cm^2. With further increase in the current density more than -100 mAcm^{-2}, the proton reduction rate is higher than the deposition of metals. Further increase in the current density only leads to an increase in the rate of hydrogen reduction which subsequently decreases the current efficiency [17, 22, 30]. It is assumed that both single metals are reduced in two consecutive steps:

$$Ni\ (II) + e^- \rightarrow Ni(I)_{ads.} \quad (7)$$

$$Ni\ (I)_{ads} + e^- \rightarrow Ni(S) \quad (8)$$

$$Fe\ (II)\ ) + e^- \rightarrow Fe(I)_{ads.} \quad (9)$$

$$Fe\ (I)_{ads} + e^- \rightarrow Fe(S) \quad (10)$$

Reduction of proton and dissociation of water molecule gives hydrogen evolution which may occur as side reactions (equation 11-13) [17, 30]. Let i_{Ni}, i_{Fe} and i_{side} are partial currents of Ni, Fe and side reaction, respectively. The total current is equal to sum of partial currents. Moreover, the change in the current efficiency is expressed by the following equation [16].

$$I_{total} = i_{Ni} + i_{Fe} + i_{side} \quad (11)$$

$$\text{Current efficiency} = i_{Ni} + i_{Fe} / i_{side} \quad (12)$$

$$H^+ + e^- \rightarrow \tfrac{1}{2}\ H_2 \quad (13)$$

$$H_2O + e^- \rightarrow 1/2\ H_2 + OH^- \quad (14)$$

$$H_2O \rightarrow H^+ + OH^- \quad (15)$$

Anodization of the Alloy

Electrochemical oxidation of $NiFe_2$ alloy films prepared at the optimum electrodeposition synthesis parameters was carried out at room temperature (25 ^{0}C) according to the conditions summarized in Table.

Table. **Conditions of the anodization process for the synthesis of Nickel ferrite thin film**

Conditions	Items
1 M KOH	Electrolyte
10	Anodic current density (mA/cm^2)
5	Intercalation time (min)
25	Electrolyte temperature (^{0}C)

The conversion of MFe_2 alloy to the corresponding ferrite (MFe_2O_4) via the hydroxide form can be explained with the following reaction

$$MFe_2 + 8OH^- \rightarrow MFe_2O_4 + 4H_2O + 8e^- \quad (16)$$

After oxidation, the hydroxide films were washed with deionized water and preserved in desiccators. Then, annealing of the hydroxide converted into the corresponding oxide (ferrite) should remove some of the defects, which may be presented during the electrodeposition and anodization steps, such as voids, grain boundaries, dislocations, stresses, in homogeneity, etc. Thus, annealing is a process related to the stress relief and local structural rearrangements resulting in recovery of alloy elements ratio in the film [22]. The formed $NiFe_2$ hydroxide precursors were annealed at 400 ^{0}C for 2 h. After annealing, a sharper and more intense diffraction peak due to the (311) plan (expected for spinel structure) is observed. This observation suggested that the nucleation of a spinel phase was formed after anodization and the crystallization process was completed after annealing [22].

Physical characterization of Ni Fe_2O_4 film

Crystal structure

The XRD pattern of nickel ferrite thin film prepared at current density - 100 mA cm^{-2} is shown in Fig. 10. Figure 10 describes the formation of well crystallite $NiFe_2O_4$ phase. Peaks at 2θ of 35.44°, 43.14°, 56.84°, 62.52°, 65° related to XRD diffraction planes (311), (400), (422), (440), and (531) were presented. These peaks confirmed that cubic spinel nickel ferrite (JCPDS#01-071-3850) was formed in a well crystalline form. The sharpness of XRD peaks was essentially attributed to the small diameter size of the $NiFe_2O_4$ film. From the main diffraction peaks and Scherer equation. The average size of crystallites for $ZnFe_2O_4$ from the most intense peak (311) based on Scherer's equation. The average crystalline size was found to be about 16 nm taking coefficient k = 0.9, proves that the films are nanocrystalline. The crystallite size was calculated automatically by the X –ray diffractometer.

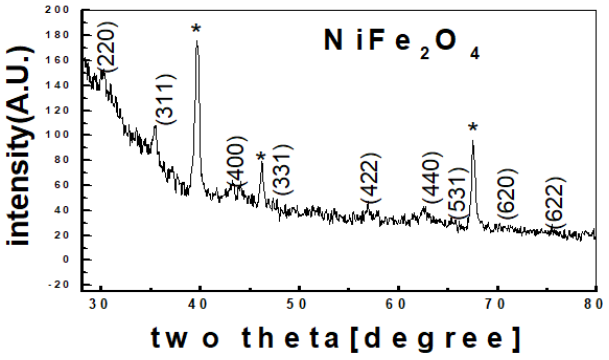

Fig. 10. XRD patterns of $NiFe_2$ alloy electrodeposited from sulfate bath at current density -100mAcm^{-2} deposited from solution of 0.1 M Fe $(NH_4)_2$ $(SO_4)_2$ + + 0.05M $NiSO_4$

Microstructure

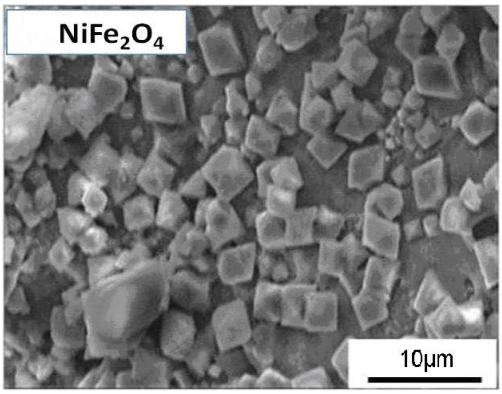

Fig. 11. SEM image of Nickel ferrite thin film electrodeposited from sulfate bath at current density -100mAcm^{-2} deposited from solution of 0.1 M Fe $(NH_4)_2$ $(SO_4)_2$ + 0.05M $NiSO_4$

Figure 11 illustrates the SEM morphology of the surface of nickel ferrite electrodeposted from sulphate bath at cathodic current density 100 mA cm^{-2}. The deposited film was subjected to microscopic examination at X 10.000. The micrograph shows compact crystallites shapes with particles and chains formed with smallest particle size. It was also observed that the distorted rectangular structure and semi square like morphology was noted.

Conclusions

The results can be summarized as follows:

- Nickel ferrite has been successfully synthesized via a novel approach of electrodeposition – anodization process
- Electrodeposited $NiFe_2$ alloy was formed from aqueous sulphate bath at a cathodic current density 100 mAcm^{-2} with a high current efficiency 82%.
- The formed alloy was anodized in 1 M KOH to form nickel ferrite precursors which annealed at 400 ^{0}C for 2 h.
- The results revealed that agitation effect had enhanced effect on current density but had opposite effect on film adhesion
- The results also revealed that bath temperature had strong promoting effect on nickel –iron alloy deposition.
- Chronoamperometric curves showed that a higher application of constant current leads to a higher potential plateau during film deposition**.**
- As the deposition current increases the thickness of the deposited film increases and optimum current efficiency satisfied at cathodic current density 100 mA cm^2.
- According to XR patterns the prepared film was nickel ferrite with spinel crystal structure, the crystallite size was 16nm predicted the film was nanocrystalline.
- According to theoretical SH model it is observed that the nucleation and growth mechanism prevailed experimentally instantaneous nature at lower and higher potentiostatic condition from -1V to -1.4V.
- According to SEM micrographs, the prepared film was homogeneous uniform and well covering the substrate. It is distorted rectangular structure and semi square like morphology.

References

1. Nabiyouni G, Fesharaki M Jsfari, Mozafari M, Amighian J (2010) Characterization and Magnetic Properties of Nickel Ferrite Nanoparticles Prepared by Ball Milling Technique chin phys lett 27:126401

2. Rodrigues ARO, Gomes IT, Almeida BG ,Araújo JP ,Castanheira Elisabete MS, Coutinho J G Paulo (2015) Magnetic liposomes based on nickel ferrite nanoparticles for biomedical applications Phys Chem Chem Phys17:18011-18021

3. Umapathy G ,Senguttuvan G, Berchmans LJ (2014) Investigation on Combustion Synthesis of Nanocyrstalline Nickel Ferrite Using Sodium Azide as a Potential Fuel Int J of Chem Tech Research 01: 131-13707

4. Wang W, Ding Z, Zhao X, Wu S, Li F, Yue M, Liu Ping http://scitation.aip.org/search?Value1=J.+Ping+Liu&option1=author&option912=resultcategory&value912=researchpublicationcontent(2015) Microstructure and magnetic properties of mfe_2o_4 (M = Co, Ni, and Mn) ferrite nanocrystals prepared using colloid mill and hydrothermal method. J Appl Phys 117: 17A328

5. AMIRI GR, YOUSEFI MH, ABOLHASSANI MR, MANOUCHEHRI S, KESHAVARZ MH, FATAHIAN S (2011) MAGNETIC PROPERTIES AND MICROWAVE ABSORPTION IN NI-ZN AND MN-ZN FERRITE NONOPARTICLES SYNTHESIZED BY LOW-TEMPERATURE SOLID-STATE REACTION. JOURNAL OF MAGNETISM AND MAGNETIC MATERIALS323: 730-734

[6. Yallapu MM, Othman SF, Curtis ET, Gupta BK, Jaggi M, Chauhan SC (2011) Multi-functional Magnetic Nanoparticles for Magnetic Resonance Imaging and Cancer Therapy. Biomaterials32: 1890-1905

7. Sertkol M, Koseoglu Y, Baykal A, Kavas H, Bozkurt A, Toprak M S (2009) Microwave synthesis and characterization of Zn-doped nickel ferrite nanoparticles. J Alloys Compd 486: 325–329

8. Jiny-H, Seo SD, Shim HW, Park KS, Kim D (2012) Synthesis of core/shell spinel ferrite/carbon nanoparticles with enhanced cycling stability for lithium ion battery anodes, jop science Nanotechnology, Vol 23

9. Lazarević Z Ž, Jovalekić Č, Milutinović A, Sekulić D, Slankamenac M, Romčević M, Romčević NŽ (2013) Study of $nife_2o_4$ and $znfe_2o_4$ Spinel Ferrites Prepared by Soft Mechanochemical Synthesis. Ferroelectrics 448: 1-11

10. Tudorache F, Rezlescu E, Popa PD, Rezlescu N (2008) the effect of additives and sintering temperature

on the structure and humidity sensitivity of a spinel ferrite. Journal of optoelectronics and advanced materials 10:2386-2389.

11. Deraz NM, Alarifi A (2012) Microstructure and Magnetic Studies of Zinc Ferrite nanoparticles. International Journal of electrochemical science7:6501 - 6511

12. Tu, YJ, You CF, Chang CK, Wang SL (2013) Adsorption behavior of As (III) onto a copper ferrite generated from printed circuit board industry. Chemical engineering journal225:433–439

13. CHEN D, YI X, CHEN Z, ZHANG Y, CHEN B, KANG Z (2013) SYNTHESIS OF $COFE_2O_4$ NANOPARTICLES BY A LOW TEMPERATURE MICROWAVE-ASSISTED BALL-MILLING INTERNATIONAL JOURNAL OF APPLIED CERAMIC TECHNOLOGY 11

14. Bilovol V, Pampillo LG, Saccone FD (2014) Study on target–film structural correlation in thin cobalt ferrite films grown by pulsedlaser deposition technique. Thin Solid Films562:218–222

15. Li L-Z, Yu Z, Lan Z-W, Sun K, Guo R-D (2014) Effects of annealing temperature on the structure and static magnetic properties of niznco ferrite thin films. J magnmagn Mater368:8–11

16. Lokhande CD, Muller M, Kulkarni SS, Mane RS, Han S (2007) Copper ferrite thin films: single-step non-aqueous growth and properties. Journal of Crystal Growth, 303: 387–390

17. Moharam MM (2011) Electrochemical preparation of nano-crystalline ferrites films suitable for electronic applications msc Thesis Al-Azhar University Egypt

18. Xia A, Zuo C, Chen L, Jin C, Lv Y (2013) Hexagonal $srfe_{12}o_{19}$ ferrites: hydrothermal synthesis and their sintering properties. J Magn Magn Mater 332:186–191

19. Elsayed EM , Rashad MM , Khalil HFY, Ibrahim IA, Hussein MR , El-Sabbah MMB (2016) The effect of solution ph on the electrochemical performance of nanocrystalline metal ferrites mfe_2o_4 (M=Cu, Zn, and Ni) thin filmsapplnanosci6, 4:485–494

20. Takayama A, Okuya M, Kaneko S (2004) Spray pyrolysis deposition of nizn ferrite thin films. Solid State Ionic172: 257–260

21. Chavana SM, Babrekarc MK, Moreb SS, Jadhavc KM (2010) Structural and optical properties of nanocrystalline Ni-Zn ferrite thin films. Journal of Alloys and Compounds, 507: 21–25

22. Saba AE, Elsayed EM, Moharam MM, Rashad MM, Abou-Shahba RM (2011) Structure and magnetic properties of $ni_xzn1\text{-}x\ Fe_2O_4$ thin films prepared through electrodeposition method. Journal of Materials Science 46:3574–3582

23. Kumar A, hari C, Singh VB (2014) Structure and Properties of Electro Co-Deposited Ni-Fe/zro_2nano-composites from Ethylene Glycol Bath. International Journal of Electrochemical Science 9:7021 – 7037

24. YOSHIDA T, KOMATSU D, SHIMOKAWA N, MINOURA H (2004) MECHANISM OF CATHODIC ELECTRODEPOSITION OF ZINC OXIDE THIN FILMS FROM AQUEOUS ZINC NITRATE BATHS. THIN SOLID FILMS451: 166–169

25. Elsayed EM, Shalan AE, Rashad MM (2014) https://scholar.google.es/citations?User=S5EX_AEAAAAJ&hl=en&oe=asciipreparation of zno nanoparticles using electrodeposition and co-precipitation techniques for dye-sensitized solar cells applications. Journal of Materials Science: Materials in Electronics, 25:3412-3419

26. Elsayed EM, Shounoda AY, Saba AE (2011) A study on the electro-synthesis of zinc oxide films. Steel grips Surface technology, 9: 201-206

27. DONG C, WANG G, GUO D, JIANG C , XUE D HTTP://WWW.NCBI.NLM.NIH.GOV/PUBMED/?TERM=XUE%20D%5BAUTH%5D(2013) GROWTH, STRUCTURE, MORPHOLOGY, AND MAGNETIC PROPERTIES OF NI FERRITE FILMS. NANOSCALE RES LETT 8:196

28. Yin KM, Lin BT (1996) Effects of boric acid on the electrodepositionof iron, nickel and iron-nickel, Surface and coatingstechnology. 78: 1–3: 205–210

29. INAMDAR AI, MUJAWAR SH, SADALE SB, SONAVANE AC, SHELAR MB, SHINDE PS, PATLIL PS (2007) ELECTRODEPOSITED ZINC OXIDE THIN FILMS: NUCLEATION AND GROWTH MECHANISM. JOURNAL OF MATERIALS CHEMISTRY, 91: 864–870

30. ELSAYED EM, SABA AE (2009) PREPARATION OF STANDARD COPPER FERRITE THIN FILM FROM AQUEOUS SOLUTION JOURNAL OF STEEL AND RELATED MATERIAL. STEEL GRIPS, 7:137-141

* * *

Синтез нанокристаллических пленок феррита никеля из водного раствора сульфатов методом электроосаждения – анодирования: материал для выявления утечки токсичных бытовых газов и мониторинга здоровья

Е. М. Элсайед, Центральный институт исследования и развития в области металлургии, Хелван, Египет
М. М. Рашад, Центральный институт исследования и развития в области металлургии, Хелван, Египет
М. М. Мохарам, Центральный институт исследования и развития в области металлургии, Хелван, Египет
М. Р. Хуссейн, кафедра Химии, Естественнонаучный факультет, Университет Аль-Ахзар, Наср, Египет
М. М. Б. Эль-Сабба, кафедра Химии, Естественнонаучный факультет, Университет Аль-Ахзар, Наср, Египет
И. А. Ибрагим, Центральный институт исследования и развития в области металлургии, Хелван, Египет

В данной работе была исследована тонкая пленка нанокристаллического феррита никеля $NiFe_2O_4$, синтезированная методом электроосаждения-анодирования. Электроосажденные сплавы $NiFe_2$ получали из водной сульфатной ванны. В водном (1 М КОН) растворе при комнатной температуре данные сплавы подвергали электрохимическому

оксидированию (анодированию) до соответствующих гидроксидов и затем выдерживали на воздухе при 400 °C в течение 2 часов. Были оптимизированы следующие параметры, влияющие на электроосаждение сплавов $NiFe_2$: температура ванны, методика перемешивания и плотность тока. Кристаллическая структура, размеры кристаллов и микроструктура полученных ферритов были исследованы методами рентгенодифракции и сканирующей электронной микроскопии. Рентгенодифракция показала, что $NiFe_2O_4$ имеет структуру шпинели, и размер кристаллов составляет 16 нм. Сканирующая электронная микроскопия полученных ферритовых частиц показала наличие искаженной прямоугольной структуры и полуквадратичной морфологии.

Ключевые слова: феррит никеля, электроосаждение, анодирование, тонкая пленка, циклическая вольтамперометрия, наночастицы.

Получено: 04.06.18